



Journal of Aerospace Technology and
Management

ISSN: 1984-9648

secretary@jatm.com.br

Instituto de Aeronáutica e Espaço
Brasil

Ferrapontoff Lemos, Mauricio; Mussbach, Günter; Bohn, Manfred August
Evaluation of Filler Effects on the Dynamic Mechanical Behavior of HTPB-Elastomer Used
as Binder in Exemplary Composite Formulations
Journal of Aerospace Technology and Management, vol. 9, núm. 3, julio-septiembre,
2017, pp. 379-388
Instituto de Aeronáutica e Espaço
São Paulo, Brasil

Available in: <http://www.redalyc.org/articulo.oa?id=309452133009>

- How to cite
- Complete issue
- More information about this article
- Journal's homepage in redalyc.org

redalyc.org

Scientific Information System

Network of Scientific Journals from Latin America, the Caribbean, Spain and Portugal

Non-profit academic project, developed under the open access initiative

Evaluation of Filler Effects on the Dynamic Mechanical Behavior of HTPB-Elastomer Used as Binder in Exemplary Composite Formulations

Mauricio Ferrapontoff Lemos¹, Günter Mussbach², Manfred August Bohn³

ABSTRACT: This study aims to evaluate the dynamic mechanical properties of a binder, used in composite propellants, with increasing amount of different solid fillers. Dynamic Mechanical Analysis (DMA) is performed to determine the region of glass-rubber transition temperature (T_g). Further parameters were obtained from the description of the loss factor curves ($\tan\delta$) with models based on exponentially modified Gauss (EMG) distribution function. Polyurethane binders employing the polyol HTPB and diisocyanate were filled with 20, 40, and 60 mass-% of ammonium perchlorate (AP), aluminum (Al) or cyclotrimethylene trinitramine (RDX) particles, using fine and coarse mean sizes. A special turning device manufactured by Fraunhofer ICT was installed inside the curing oven in order to avoid sedimentation during curing. The cured composites were characterized by DMA in torsion mode from -100 °C to 70 °C. The good homogeneous distribution of fillers in the samples was evaluated by computational X-ray micro-tomography. The data on $\tan\delta$ showed a complex structure describable at first with 2 overlapping peaks. The peak at lower temperatures is due to mobility of unrestricted binder parts ($T_{g,unr}$) and the second broader peak at high temperature is due to mobility of restricted binder parts ($T_{g,res}$). Results of $\tan\delta$, calculated areas of EMG curves and apparent activation energies of the distinct relaxation processes indicate that Al particles have higher interaction with HTPB-based polyurethane than AP and RDX. Probably Al is bonded to the binder network via isocyanate coupling with OH groups present in the surface. Ammonium perchlorate and cyclotrimethylene trinitramine particle sizes and its morphology influenced the viscoelastic properties. AP and RDX cause more changes in intensity of first peak of loss factor than Al. Increasing amount of these both particles enhances storage (G') and loss (G'') shear moduli. As a whole $\tan\delta$ intensity is lowered in the main peak and Al showed an intensity increase in the second apparent peak.

KEYWORDS: DMA, Ammonium perchlorate, Aluminum, Cyclotrimethylene trinitramine, HTPB loss factor modelling.

INTRODUCTION

A composite solid propellant (CSP) is an energetic material characterized by the release of high amount of energy during burning, generating hot gases and low molar mass molecules (Davenas 1993; Kubota 2007; Cerri *et al.* 2009). The CSP consists of a polymer matrix (binder) containing a high amount of solid particles. Polybutadiene-based polyols such as hydroxyl-terminated polybutadiene (HTPB) are today the main pre-polymers used for CSP, which are cross-linked with polyisocyanates to give a polyurethane elastomer (Cerri *et al.* 2009; Hufferd and Fitzgerald 1976). The main solid particles used as fillers are oxidizers, such as nitrates and perchlorates, which supply oxygen for the combustion reactions. Another important filler is the aluminum powder, which acts as fuel during the combustion by its strong exothermic oxidation reaction and cyclotrimethylene trinitramine (RDX) particle that can be used in some specific HTPB-based formulations as well as in plastic bonded explosives (PBX) (Davenas 1993; Kubota 2007; Cerri *et al.* 2009; Hufferd and Fitzgerald 1976; Lemos and Bohn 2016). The binder main functions are to give dimensional stability and viscoelastic properties, assuring structural integrity to CSP and minimizing or even avoiding combustion instabilities (Davenas 1993; Kubota 2007; Hufferd and Fitzgerald 1976).

The mechanical properties of composites with elastomeric binders depend strongly on the surrounding temperatures and on the deformation frequency of the applied mechanical load. In terms of low temperature properties, the elastomer

¹Instituto de Pesquisas da Marinha – Grupo de Tecnologia de Materiais – Rio de Janeiro/RJ – Brazil. ²Bayern-Chemie GmbH – Aschau am Inn – Germany. ³Fraunhofer Institute for Chemical Technology – Pfinztal – Germany.

Author for correspondence: Mauricio Ferrapontoff Lemos | Instituto de Pesquisas da Marinha – Grupo de Tecnologia de Materiais | Rua Ipiru, 2 – Cacaia | CEP: 21.931-095 – Rio de Janeiro/RJ – Brazil | Email: mauricio.lemos@marinha.mil.br

Received: Sept., 12, 2016 | **Accepted:** Jan., 21, 2017

must be able to purvey a very low glass-rubber transition temperature (T_g) for safe operation (Davenas 1993; Kubota 2007; Cerri *et al.* 2009; Hufferd and Fitzgerald 1976; Lemos and Bohn 2016; Fluke 1969; Bohn 2016; Bohn *et al.* 2014; Cerri and Bohn 2010; Cerri *et al.* 2013). The loss factor ($\tan\delta$) as function of temperature, obtained in DMA, defines the region of glass-rubber transition. The glass-rubber transition temperature T_g is defined as temperature at the maximum in loss factor curve. However, the $\tan\delta$ curve of CSP consists of several sub-transitions referring to different fractions of the elastomer binder with different mobility (Cerri *et al.* 2009; Bohn 2016; Bohn *et al.* 2014; Cerri and Bohn 2010; Cerri *et al.* 2013; Azoug *et al.* 2015). A modeling of the loss factor curve with suitable distribution functions is needed to separate these effects in $\tan\delta$ and to characterize them quantitatively in terms of the maximum peak temperatures and by other parameters as areas (intensities), peak widths, and peak skewness (Bohn 2016; Bohn *et al.* 2014; Cerri and Bohn 2010; Cerri *et al.* 2013; Azoug *et al.* 2015).

A CSP grain is subjected to several dynamic mechanical load stresses during transport, ignition and even during storage in a broad temperature range. In several investigations the viscoelastic response is reported under dynamic loads at frequencies from 0.1 up to 110 Hz from -40°C to 50°C (Hufferd and Fitzgerald 1976). Deformation frequency of applied stress or strain imparts changes in mechanical response of a viscoelastic binder, especially in the T_g region (Cerri *et al.* 2009; Hufferd and Fitzgerald 1976; Bohn *et al.* 2014; Cerri *et al.* 2013; Ornaghi Jr *et al.* 2010). Previous study showed an undesirable δ intensity increase and a shift of the peak to higher temperatures with increasing deformation rate in CSP, caused by molecular frictions, thus indicating the possibility of high energy dissipation and therefore a heating up of the material (Bohn 2016; Bohn *et al.* 2014; Cerri *et al.* 2013). These effects have severe implications for these materials already at moderate low temperatures. It is important to evaluate to which extend each type of solid particle in a CSP formulation affects these relaxations and dissipative effects, since each particle has different interaction possibilities with the binder. This paper aims at a first step of investigation to find out how the individual fillers interact with the HTPB-based matrix. Experimental investigation is performed in order to evaluate the influence of the type of fillers on the shape and intensity of loss factor and on its shift with deformation frequency.

METHODOLOGY

SAMPLE PREPARATION

The composite samples consisted of a polyurethane binder filled with 20, 40 or 60 mass-% of different filler types. The polyurethane was obtained by the reaction of the polyol Hydroxyl-Terminated Polybutadiene type HTPB R45 HTLO (Sartomer, Polybd, Oakland, USA) with the curing agent Isophorone Diisocyanate – IPDI (Evonik, Marl, Germany) in a ratio of NCO to OH groups (R_{eq}) adjusted to 0.85. Plasticizer Dioctyl Adipate – DOA (BASF, Ludwigshafen, Germany) was added in 5 mass-% relative to total binder content. As fillers were used the ammonium perchlorate (AP), with particle size $d(0.5)$ equal to $42.83\ \mu\text{m}$ (fine) and $202.28\ \mu\text{m}$ (coarse); RDX from Dyno/Norway with $60.86\ \mu\text{m}$ (fine) and $233.26\ \mu\text{m}$ (coarse); and Al (Toyol, USA) with $d(0.5)$ of $20.69\ \mu\text{m}$ (type X81, fine) and $130.25\ \mu\text{m}$ (coarse). The composite samples were manufactured at Fraunhofer ICT in a planetary centrifugal vacuum mixer (Thinky Corporation, Tokyo, Japan). Operational conditions were 1,600 rpm rotation speed and 3 kPa vacuum during few minutes of mixing time. The temperature in the mix was kept below 40°C . The formulations were produced in small batches and poured into a cylindrical glass recipient, sealed and cured in air at 60°C for 96 h. The binder was protected by the addition of the antioxidant Vulkanox™ BKF.

Just after mixing, the particles were homogeneously distributed all over the sample volume. However, the particles tended to sediment in the liquid binder mix in early stages of the curing process, when the viscosity was not yet high. This problem was even more critical for samples with lower amounts of solid loading, such as 20 and 40 mass-% of fillers. Thus, in order to keep the fillers homogeneously distributed during all stages of curing process, a special turning device was manufactured at Fraunhofer ICT and installed inside the curing oven (Fig. 1).

The turning machine was optimized to work safely with explosive materials. It provides a rectangular frame for adapting samples within a standard laboratory circulation oven UFE500 (Mettmert, Germany). The frame was rotated not permanently to avoid distribution gradients of the filler particles due to inertia forces. It was rotated stepwise by 180 degrees, controlled by encapsulated, low-voltage magnetic switches. A belt drive in combination with a screw wheel transmission was powered by a brushless AC-motor. An additional transmission was necessary for suppressing rattle-effects. The switches and the motor were connected to a programmable electronic circuit, which allows controlling the rotation speed and the holding time. The circuit

was equipped with a counter to monitor the number of rotation cycles, useful for instance in case of failures in power network. The turning time is typically about 4 s and the holding time was set to 60 s. After curing, the glasses were broken and the DMA samples cut from the middle of the cured composite.

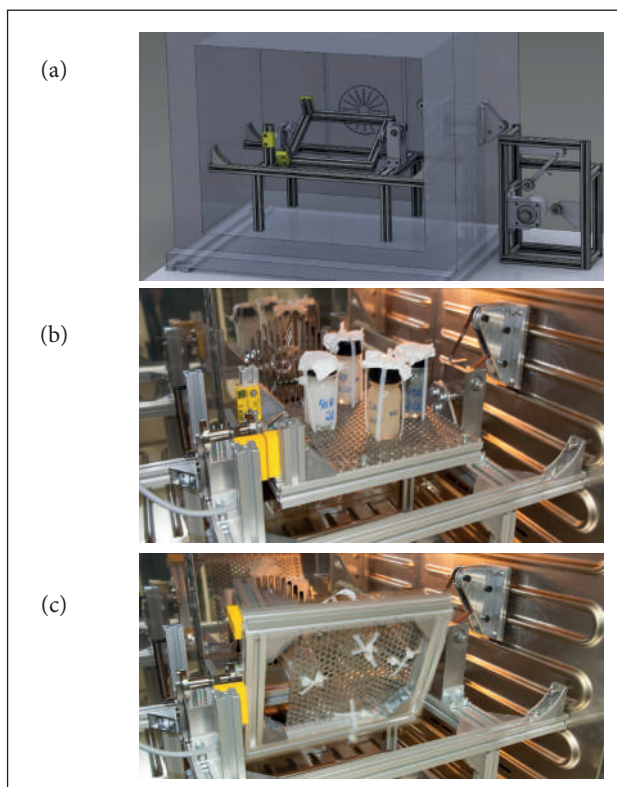


Figure 1. Design of the turning machine, schematic sketches (a). Installation and operation in curing oven shown in photographs (b and c) at Fraunhofer ICT. The device was used successfully for the curing of elastomers with low degree of filling of solid particles to avoid sedimentation.

SAMPLE CHARACTERIZATION

A microcomputer tomography Micro-CT in-vivo Skyscan 1076 (Bruker, Germany) was used to evaluate the distribution of the fillers in the samples taken for DMA measurements.

Dynamic mechanical analysis measurements in torsion mode were carried out with a DMA ARESTM (Advanced Rheometric Expansion System) manufactured by the former Rheometric Group of the company Rheometric Scientific, Inc. (this group belongs now to Waters, Inc., BU TA Instruments, New Castle, NJ, USA). The following parameters were determined: storage shear modulus G' , loss shear modulus G'' , loss factor $\tan \delta = G''/G'$ as well as the phase angle δ and the torque. Measurements were performed in torsion mode from -100°C

to $+70^\circ\text{C}$, with heating rate of $1^\circ\text{C}/\text{min}$ and soak time of 28 s. At -100°C a pre-strain sweep test was performed to determine the value of strain control, in order to stay in the linear viscoelastic region during the measurements. At each temperature step, the specimens were measured at 4 sinusoidal deformation frequencies (0.1; 1; 10 and 30 Hz). The geometrical dimensions of the rectangular samples were about 40 mm length, 10 mm width and 5 mm thickness. In the cases where the material was too soft (as with pure binder and binder with 20 and 40 mass-% of filler), the signal scattered and a second strain sweep was necessary at -40°C to determine a higher second strain control to be used from about -40°C up to $+70^\circ\text{C}$.

Scanning electron microscopy (SEM) images were obtained by Supra 55VP (Zeiss, Germany).

RESULTS AND DISCUSSIONS

In Fig. 2, a sample with 20 mass-% of AP was used to show how the particles are homogeneously distributed in the elastomers after curing using the turning machine. The Micro-CT X-ray scan, shown in Fig. 2b, demonstrates the homogeneity of the distribution of the AP particle.

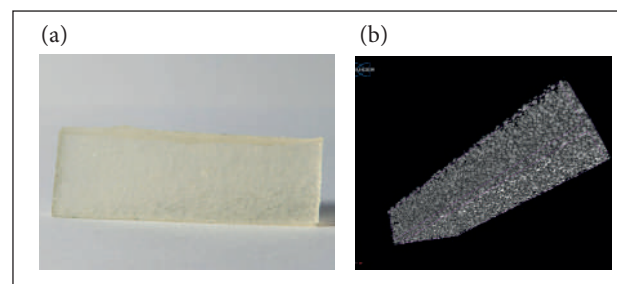


Figure 2. Images from DMA sample with 20 mass-% of AP. (a) Normal optical photograph and (b) 3-D image taken from a Micro-CT X-ray scan, showing AP particles in gray.

At first and to model the loss factor curves, a suitable base line correction (BLC) was applied to separate the part standing for only dissipation of applied deformation energy (Bohn 2016; Bohn *et al.* 2014; Cerri and Bohn 2010) from the part containing information on the molecular rearrangement processes in going from energy elastic to entropy elastic state. Further, the modeling allows then to separate the binder contributions to the loss factor curve in terms of differences in mobility of binder molecules and to quantify the influence of fillers on the loss factor. In Fig. 3, the base line corrected

loss factor curves at all deformation frequencies are shown for the samples with increasing amount of AP, RDX and Al. Each sample has 2 apparent peaks, with tailing towards higher temperatures. Table 1 shows the values of T_g for each $\tan\delta$ peak for each frequency. The values of the differences between the T_g of composite and of pure binder are taken as reference

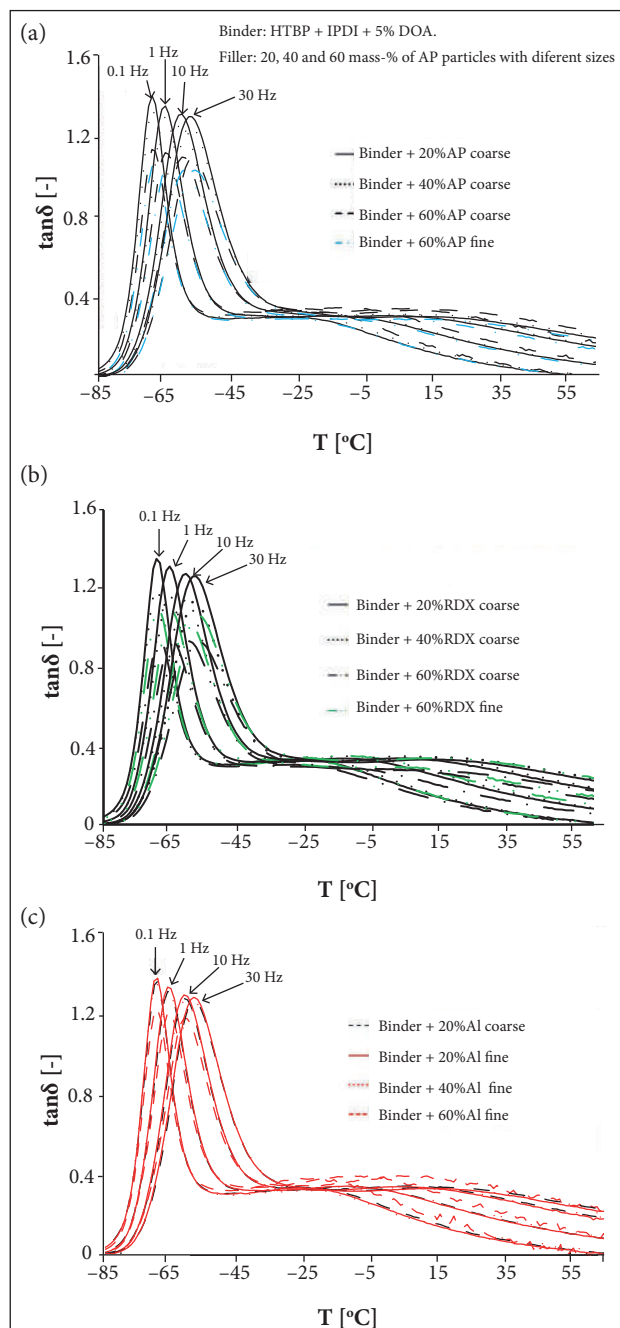


Figure 3. Deformation frequency dependence of the loss factor curve of composites samples with 20, 40, and 60 mass-% of AP (a), RDX (b) and Al (c) fine and coarse particles.

and are also presented. Samples with 60 mass-% of RDX had no defined apparent second peak in loss factor curves at deformation frequency higher than 0.1 Hz. This is a general feature also shown with HMX as filler (Bohn *et al.* 2014).

The first peak at lower temperatures represents the “mobility unrestricted glass-rubber transition” with the temperature T_g^{unr} , and it is attributed to the main transition of the soft segment regions of the HTPB chains in the temperatures range of -80 to -60 °C. The second broader peak originates from the transition regions of the hard segments of the polyurethane network (cross-link sites) and in part of the binder molecules (soft and/or hard segments), which have restricted mobility, for example, by filler-binder interaction. Therefore, this peak is called “restricted” and the associated maximum temperature is named T_g^{res} (Cerri *et al.* 2009; Bohn 2016; Cerri *et al.* 2013; Azoug *et al.* 2015). Each transition region corresponds to molecular rearrangements of fractions of the binder with different mobility. T_g^{unr} increased slightly at higher temperatures by increasing the amount of AP and RDX particles but this decreased more considerably the $\tan\delta$ intensity of the first peak especially at higher frequencies of applied strain. In Fig. 4, the curves are shown comparing loss factor curves at frequencies of 0.1 and 30 Hz. The curves of the samples with 60 mass-% of AP, RDX, and Al (fine) are indicated. Despite having less effect on the first peak, the Al addition imparts more intensity to $\tan\delta$ of the second peak, and also shifted it to higher temperatures (see T_g^{res} values of the lines of 60 mass-%-filled samples in Table 1). A distinguishable

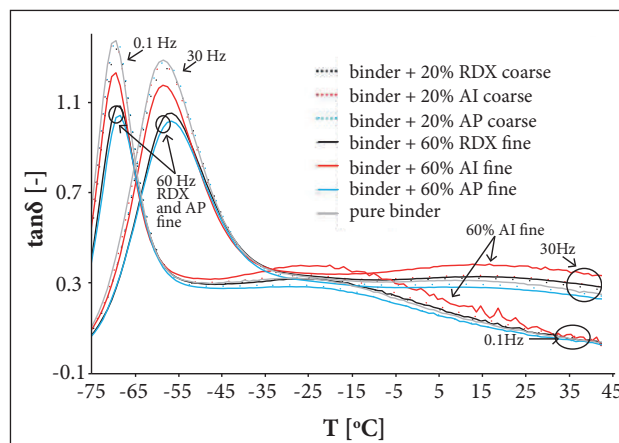


Figure 4. Loss factor curves of pure binder and of composites samples with 20 and 60 mass-% of AP, RDX, and Al coarse and fine particles. DMA in torsion mode at frequencies of 0.1 and 30 Hz.

Table 1. Values of T_g^{unr} and T_g^{res} for the first and second peaks, respectively, of $\tan\delta$ curve, at different deformation frequencies.

Sample content mass (%)	Values of T_g^{unr} (°C) for each test frequency				Difference to reference (°C)				Ea_f^* [kJ/mol]	$\ln(f_0)$ [Hz]
	0.1 Hz	1 Hz	10 Hz	30 Hz	0.1 Hz	1 Hz	10 Hz	30 Hz		
Binder alone	-69.42	-65.58	-60.72	-57.95	Reference				180.7	45.43
20%AP coarse	-68.86	-65.24	-60.28	-57.51	0.56	0.34	0.44	0.44	182.6	45.79
40%AP coarse	-68.78	-65.04	-60.11	-57.27	0.64	0.54	0.61	0.68	180.9	45.34
60%AP coarse	-68.63	-64.76	-59.62	-56.74	0.79	0.82	1.10	1.21	175.4	43.91
60%AP fine	-68.29	-64.38	-59.06	-56.16	1.13	1.20	1.66	1.79	172.3	43.04
20%RDX coarse	-68.95	-65.02	-60.09	-57.37	0.47	0.56	0.63	0.58	179.8	45.07
40%RDX coarse	-68.97	-65.01	-59.91	-57.22	0.45	0.57	0.81	0.73	176.7	44.30
60%RDX coarse	-69.58	-64.28	-59.02	-55.94	-0.16	1.30	1.70	2.01	154.9	38.78
60%RDX fine	-69.44	-64.56	-59.19	-56.19	-0.02	1.02	1.53	1.76	158.6	39.71
20%Al coarse	-68.90	-65.65	-60.76	-57.91	0.52	-0.07	-0.04	0.04	187.3	47.05
20%Al fine	-69.54	-65.71	-60.81	-57.95	-0.12	-0.13	-0.09	0	179.1	45.00
40%Al fine	-69.23	-65.69	-60.71	-57.77	0.19	-0.11	0.01	0.18	180.6	45.34
60%Al fine	-69.01	-65.56	-60.60	-57.80	0.41	0.02	0.12	0.15	184.0	46.18
Sample content mass (%)	Values of T_g^{res} (°C) for each test frequency				Difference to reference (°C)				Ea_f^* [kJ/mol]	$\ln(f_0)$ [Hz]
	0.1 Hz	1 Hz	10 Hz	30 Hz	0.1 Hz	1 Hz	10 Hz	30 Hz		
Binder alone	-28.04	-13.65	2.52	10.87	Reference				84.7	17.06
20%AP coarse	-29.42	-15.63	2.00	11.03	-1.38	-1.98	-0.52	0.16	80.7	16.33
40%AP coarse	-28.33	-14.14	2.94	12.46	-0.29	-0.49	0.42	1.59	81.3	16.37
60%AP coarse	-24.92	-11.96	4.22	14.98	3.12	1.69	1.70	4.11	85.4	17.03
60%AP fine	-29.25	-16.82	0.23	8.49	-1.21	-3.17	-2.29	-2.38	85.2	17.31
20%RDX coarse	-25.36	-12.23	4.57	14.24	2.68	1.42	2.05	3.37	85.1	17.00
40%RDX coarse	-24.34	-10.94	6.36	15.75	3.70	2.71	3.84	4.88	84.6	16.82
60%RDX coarse	-25.38	Not well defined			2.66	Not well defined				
60%RDX fine	-24.05	-11.76	4.96	15.47	3.99	1.89	2.44	4.60	86.1	17.14
20%Al coarse	-26.01	-11.7	6.13	15.09	2.03	1.95	3.61	4.22	81.7	16.29
20%Al fine	-25.88	-12.44	3.76	13.54	2.16	1.21	1.24	2.67	85.5	17.10
40%Al fine	-25.91	-11.74	4.35	11.32	2.13	1.91	1.83	0.45	88.7	17.74
60%Al fine	-23.25	-10.33	7.38	15.8	4.79	3.32	4.86	4.93	86.5	17.14

change in the first peak with the addition of AP and RDX in comparison to Al might be related with volumetric effects. The densities of AP and RDX are 1.95 g/cm³ and 1.82 g/cm³, respectively, whereas Al has 2.7 g/cm³. So the use of an equal mass results in a higher occupied volume by the particles in the composites with AP and RDX, imparting more geometrical hindrance to chain mobility than by the Al. On the other hand, Al filled samples present a higher intensity on the second peak, which might be explained by a higher filler-binder interactions.

The molecular rearrangements during glass-rubber transition enhance the thermo-mechanical energy loss inside the polymer. Therefore, loss shear modulus increases. During glass-rubber transition, when the molecules are stimulated to pass a threshold of energy, long-range chain mobility takes place along the segments and the loss factor is at its maximum. By increasing the deformation frequency in DMA, the chains have less time to move and rearrange in order to accommodate the mechanical energy. So when heating up the samples from very low temperatures, the energy elastic

state is retained longer, up to higher temperatures. Often this effect is also named strain rate hardening.

The deformation frequency dependence of the thermo-mechanically activated glass-rubber transition can be expressed by Arrhenius parameterization. With the use of an Arrhenius type equation (Eq. 1), an apparent activation energy Ea_f^* of the distinct relaxation process can be estimated.

$$f = f_0 \cdot \exp\left(-\frac{Ea_f^*}{R \cdot T_g(f)}\right) \quad (1)$$

where: f is the applied deformation frequency [Hz]; f_0 is the apparent pre-exponential factor [Hz]; Ea_f^* is the apparent activation energy [kJ/mol]; R is the general gas constant [8.31441 J/K·mol]; T_g is the glass-rubber transition temperature [K] as function of deformation frequency f .

In Table 1 the values of Ea_f^* and f_0 are listed. In Fig. 3 the shift of the loss factor curve to higher temperatures can be seen with increasing deformation frequency for the samples with increasing amount of AP, RDX, and Al.

The Ea_f^* values of the distinct relaxation process change slightly with filler addition. With AP addition the Ea_f^* of first peak (T_g^{unr}) increases initially (20 mass-%), but then decreases with increasing amount of filler. RDX addition, however, decreases continuously the Ea_f^* of T_g^{unr} . An opposite trend is found with the values of activation energies of the T_g^{res} . The addition of Al particles imparted overall slightly higher values of Ea_f^* among all, which is an indication of higher interaction with the polymer matrix.

In Fig. 5, the elastic (storage) and loss shear modulus (G' and G'') are presented for all the samples tested at deformation frequency of 10 Hz. Before the transition, G' and G'' are very similar for the composites. Only G' of samples with 60 mass-% is significantly higher. Increasing amount of AP and RDX particles enhances G' and G'' , although with AP this happens mainly after T_g^{unr} . Al produces this effect more pronounced at lower temperatures. After the first transition the differences increase, and it is notable that the increase in solid filler content in the composites increases both G' and G'' . Storage modulus increase is related with a reinforcement of the material, whereas loss modulus increase with increasing solid fillers in composites is known to be caused by an enhanced internal friction in dynamic mechanical loading experiments (Bohn *et al.* 2014; Ornaghi Jr *et al.* 2010). Regarding particle sizes, the use of fine AP and fine RDX incremented G' more than G'' .

The quantification of the effects (interaction and amount) of each filler on the loss factor curve is possible with the use of a model based on exponentially modified Gauss (EMG) distribution functions. The EMG is a convolution between Gauss distribution and exponential decay function. Previous studies have described the model in details (Bohn 2016; Bohn *et al.* 2014; Cerri and Bohn 2010; Azoug *et al.* 2015). The application

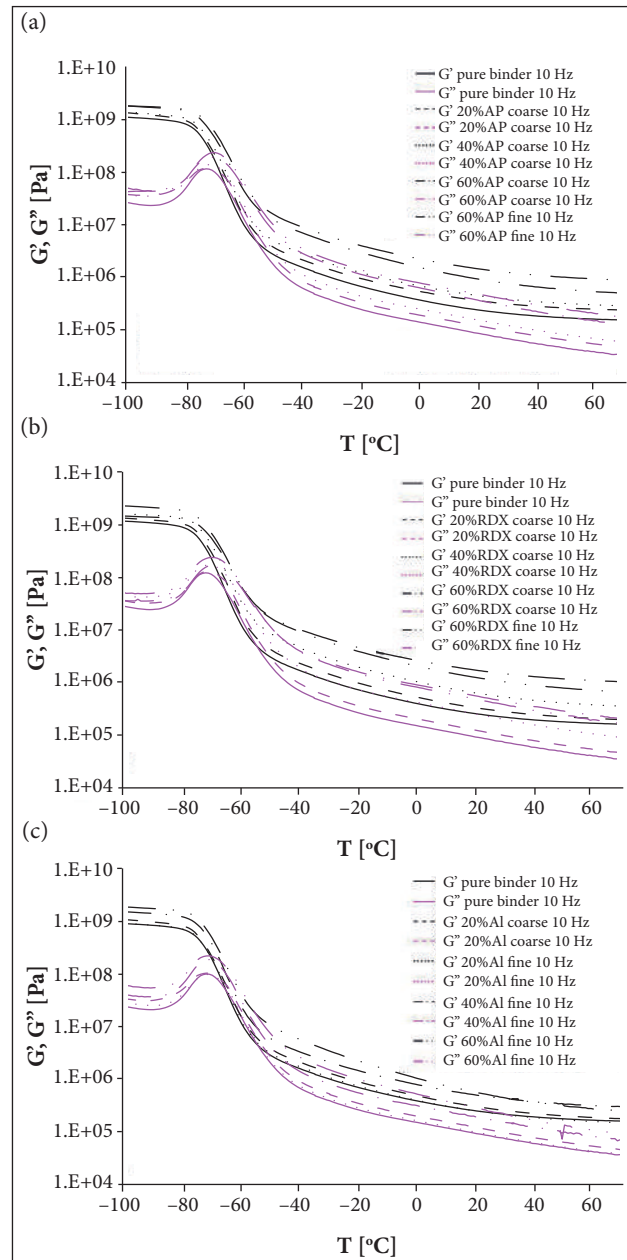


Figure 5. G' and G'' curves of all samples measured at 10 Hz deformation frequency of applied strain. Samples consisting of binder with increasing amount (20, 40, and 60 mass-%) of (a) AP, (b) RDX, and (c) Al.

of EMGs provides parameters of the sub-transition regions of the loss factor curve: the peak areas (A_i); the half peak width at half height of the Gaussian part of corresponding EMG_i (w_i); the temperature at peak maximum of Gaussian part of the EMG_i (T_{c_i}) and the relaxation parameter τ_i in the exponential part of the EMG_i (herein named To_i). Figure 6 shows 3 EMG functions to describe each of the $\tan\delta$ data of the pure binder (a) and of the composite filled with 60 mass-% of Al particles (b). This was done for all samples at all deformation frequencies. Due to limited space only the parameters obtained for the samples filled with 60 mass-% particles are presented in Table 2.

Two parameters are considered to be more important for composites and are discussed in more detail. One is the parameter A_3 , which is the area of the loss factor curve. When the intensity of the glass-rubber transition expressed by A is small, the reasons can be: (1) more hindrance in mobility for

the pre-polymer or (2) a more elastic behavior of the polymer means a more dominant elastic (storage) shear modulus. The other parameter of importance is the peak temperature T_{c_i} .

Regarding the sum of the peak areas ($\sum A_i$), filling the binder with AP coarse particles had nearly no effect. Fine AP however had caused an overall depreciation of A_i parameters. This means that the polymer gained more in the elastic than in the loss shear modulus — one can say the sample is more elastic and less viscous. RDX has a reversed effect: the filling with coarse particle size had decreased the sum of A_i parameters. SEM analysis of AP fine and RDX coarse particles (Fig. 7b and 7c) showed that both are less round (means have more irregular geometry and edges), whereas coarse AP and fine RDX (Fig. 7a and 7d) had an apparent geometry closer to a sphere or are rounded particles. This is an indicative that the sum of A_i parameters, meaning the overall area of the loss factor curve, seems more affected by the AP and RDX particle shapes than by their size.

A_3 is the area of the peak attributed to the transition of parts of the binder with more restriction to chain mobility, i.e. in filler-binder interfaces for example. It is evident from the results that the addition of Al particles had a stronger effect on increasing the value of this parameter than the other particles, and this effect is even more pronounced when deformation frequency is increased.

On the surface of aluminum particles there is the possibility of forming Al hydroxide due to contact of the metallic Al with air (oxygen) and humidity. It was already discussed in the literature that the OH on Al may capture one end of isocyanate molecules (Cerri *et al.* 2009; Cerri *et al.* 2013), leaving less isocyanate groups to react with pre-polymer and more not bonded polyol chain ends are available. This may change the R_{eq} in the binder near the Al particles. According to literature, the second apparent loss factor peak in HTPB-based solid propellants, consisting mainly by the EMG-3 (peak 3), can be caused by 2 effects:

1. From the flow of free polymer chains in the polymer network with a reptation mechanism. If more polymer or polyol chains are available to move near the particle due to isocyanate “capture” near the Al surface, one could expect an increase in A_3 value (Azoug *et al.* 2015).
2. From a more intense intermolecular interaction between Al and HTPB than between the polyol and AP. Due to stronger interactions, the Al exert more hindrance on the mobility of the HTPB chains in the polymer shell around the particles (Nardai and Bohn 2015). As a first consequence the glass-rubber transition temperature of

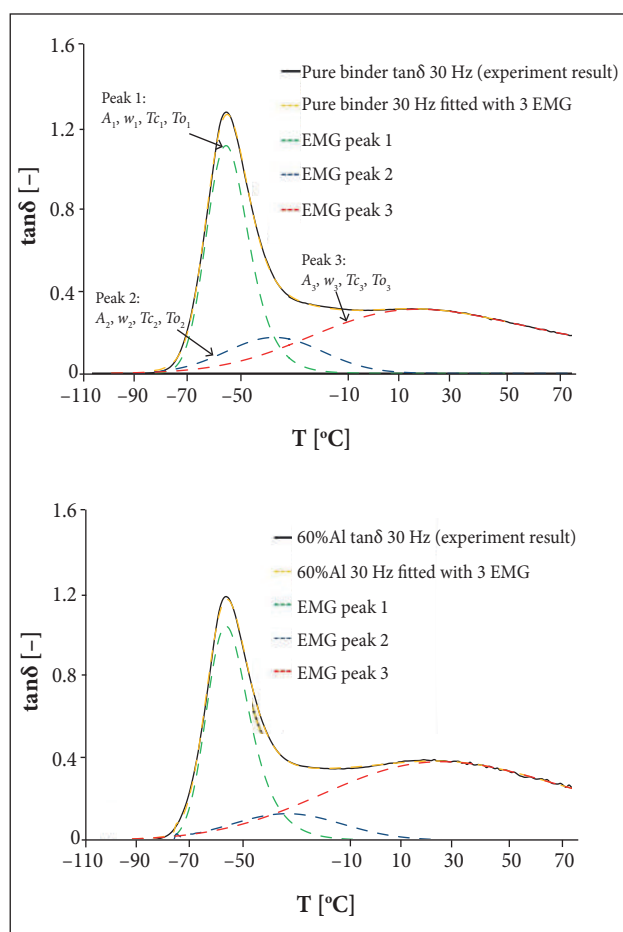


Figure 6. Description of loss factor with 3 EMG functions of the pure binder (a) and of the composite with 60 mass-% of Al (b). This resolves 3 sub-peaks or 3 binder fractions with different mobility.

Table 2. Values of EMG parameters of samples with 60 mass-% coarse and fine particles in comparison with the pure binder.

	Pure binder				60 mass-% AP coarse				60 mass-% AP fine			
f (Hz)	0.1	1	10	30	0.1	1	10	30	0.1	1	10	30
A_1	13.3	16.7	20.3	22.5	10.8	13.5	16.2	18.0	11.0	13.9	17.0	22.5
A_2	2.6	5.6	7.2	7.8	2.8	4.8	8.2	8.3	3.7	7.9	7.6	6.7
A_3	24.8	29.0	39.0	42.3	25.2	30.9	38.7	45.8	19.9	21.3	31.3	34.1
$\sum A_i$	40.8	51.3	66.5	72.7	38.8	49.3	63.2	72.2	34.5	43.1	56.0	63.3
w_1	4.2	5.2	5.6	6.3	4.3	5.2	5.6	6.3	4.5	5.5	6.1	6.7
w_2	2.0	2.7	16.4	17.5	2.1	2.8	17.0	17.5	2.3	3.1	16.5	6.6
w_3	25.3	26.3	26.7	28.5	26.8	27.7	25.5	28.1	24.7	25.6	23.9	30.6
Tc_1	-70	-66	-65	-63	-69	-66	-64	-61	-69	-65	-63	-65
Tc_2	-63	-58	-46	-43	-62	-57	-46	-42	-61	-56	-43	-57
Tc_3	-43	-33	-23	-20	-38	-32	-20	-17	-39	-28	-19	-12
To_1	0.9	1.0	5.6	6.4	0.8	1.0	5.5	6.1	0.9	1.0	5.8	23.8
To_2	9.6	17.1	2.7	3.0	11.4	16.6	3.2	3.0	15.4	26.8	3.3	1.0
To_3	22.3	37.6	60.1	70.8	17.6	35.1	59.3	75.1	20.9	34.5	57.9	66.6
	60 mass-% RDX coarse				60 mass-% RDX fine				60 mass-% Al fine			
f (Hz)	0.1	1	10	30	0.1	1	10	30	0.1	1	10	30
A_1	9.7	12.1	16.2	19.2	10.8	13.7	17.4	19.4	13.4	14.9	17.7	21.2
A_2	3.3	6.3	7.3	6.1	3.0	5.4	10.1	13.4	2.6	5.2	7.5	6.5
A_3	21.3	22.9	28.6	33.5	23.9	32.5	35.6	37.4	25.4	35.6	48.2	49.8
$\sum A_i$	34.3	41.2	52.2	58.8	37.7	51.6	63.1	70.2	41.4	55.7	73.4	77.4
w_1	4.5	5.5	6.0	6.7	4.3	5.4	6.8	7.6	4.2	5.2	5.1	6.0
w_2	2.2	3.1	17.4	17.3	2.2	3.1	4.1	4.8	1.7	2.9	21.1	20.0
w_3	25.9	27.0	23.8	27.4	26.2	26.7	31.6	34.6	25.8	27.0	30.1	34.2
Tc_1	-69	-65	-64	-62	-69	-65	-61	-58	-70	-66	-65	-63
Tc_2	-61	-57	-41	-34	-62	-57	-50	-47	-63	-58	-49	-39
Tc_3	-40	-31	-18	-14	-39	-33	-16	-5	-41	-30	-20	-11
To_1	0.8	1.0	6.8	8.2	0.8	1.0	1.4	1.5	0.8	1.0	6.6	7.5
To_2	15.5	22.4	3.3	3.2	11.6	17.9	29.3	35.5	9.9	16.0	3.0	3.1
To_3	19.7	32.8	54.4	65.3	19.3	43.3	54.6	60.1	21.0	35.8	59.3	56.6

such binder fractions is shifted to higher temperature values compared to not mobility restricted HTPB chains (see Tc_3 parameters). Secondly, because of the increased binder part in this fraction, it creates a relative intense glass-rubber transition, since the mobility restriction

imparted by Al is not high enough to avoid the transition to take place, meaning that no rigidity for the polymer chains is caused.

On the other hand, this effect of reducing mobility can be also the case, if one has increasing cross-linking between the

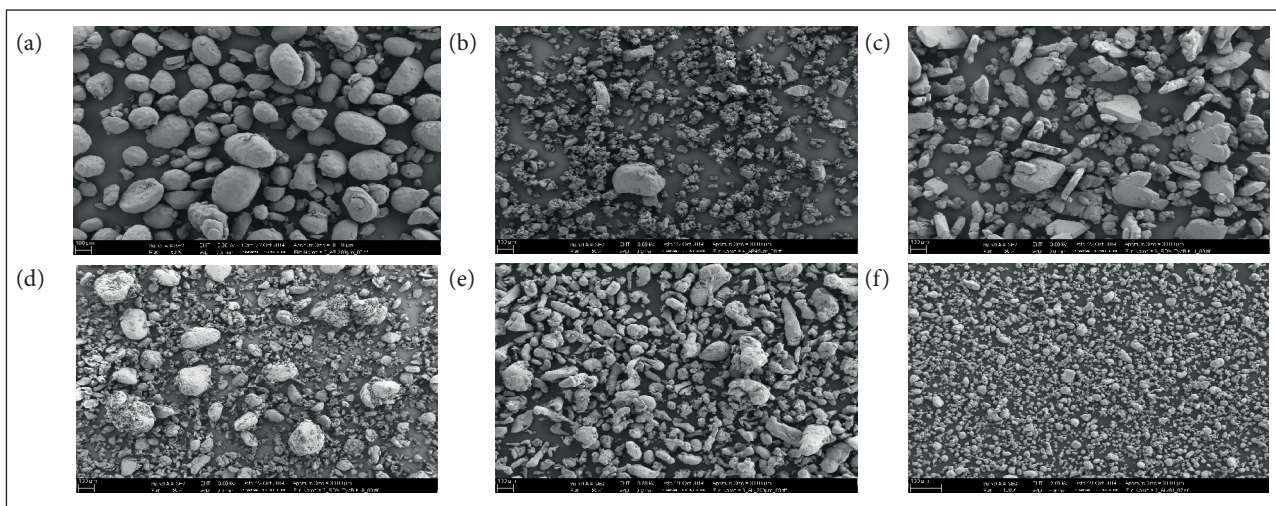


Figure 7. SEM images (magnification of 50X) of the particles loaded in the CSP in this study. (a) Coarse AP, rounded; (b) Fine AP, non-rounded [AP] particles; (c) Coarse RDX, non-rounded; (d) Fine RDX, rounded; (e) Coarse Al, rounded; (f) Fine Al, rounded. Scale of 100 μm .

polymer chains in the neighborhood of particles, which form then a more rigid amorphous region and the transition intensity is reduced, but the storage modulus increases. Another effect is the stronger chemical bonding of Al particles to the network, when isocyanate attaches to the Al surface via its OH groups. This enlarges the polymer shell around Al particles and the intensity of A_3 is increased.

Regarding the T_c parameters, T_{c1} is nearly not affected, independent of particle size or type. T_{c3} is increased, and the increase is more pronounced at higher frequencies, especially with fine particle sizes. This is an indication that an increase in solid filler tend to enhance chain mobility restrictions, affecting the T_g^{res} , corroborating the results shown in Table 1.

Results of $\tan\delta$ intensity as calculated areas of EMGs fitting curves and results of apparent activation energies of the distinct relaxation process during T_g^{res} with increasing frequency indicates that Al particles have higher interaction possibilities with HTPB-based polyurethane binder than AP and RDX, when no bonding agents are used. Probably Al is bonded to the binder network via isocyanate coupling, because on Al surfaces OH groups are always present. AP and RDX particle sizes and their shape or their particle morphology influence the viscoelastic properties. Increasing amount of AP and RDX particles enhances storage (G') and loss (G'') shear moduli, but AP causes this effect mainly during and after T_g^{unr} . Al produces this effect more pronounced at lower temperatures in the range of the second loss factor peak.

CONCLUSIONS

AP and RDX impart more changes in $\tan\delta$ intensity of the first loss factor peak than Al particles. The main glass-rubber transition temperature (T_g^{unr}) is nearly not affected by the addition of particles.

AUTHOR'S CONTRIBUTION

Lemos MF and Mussbach G performed the experiments; Lemos MF and Bohn MA conceived the ideas and co-wrote the main text. All authors discussed the results and commented on the manuscript.

REFERENCES

Azoug A, Nevière R, Constantinescu A (2015) Molecular origin of the influence of the temperature on the loss factor of solid propellant. *Propellants Explos Pyrotech* 40(4):469-478. doi: 10.1002/prep.201400060

Bohn MA (2016) Influences on the loss factor of elastomer binder for composite materials and its modelling. *Proceedings of the 3rd Brazilian Conference on Composite Materials*; Gramado, Brazil.

Bohn MA, Mußbach G, Cerri S (2014) Modeling of loss factors of elastomer binders of high explosive charges and composite rocket propellants to separate binder fractions with different molecular mobility used to follow aging. Proceedings of 10th International Symposium on Special Topics in Chemical Propulsion & Energetic Materials; Poitiers, France.

Cerri S, Bohn MA (2010) Separation of molecular mobility ranges in loss factor curves by modeling with exponentially modified gauss distributions. Proceedings of the 41st International Annual Conference of ICT; Karlsruhe, Germany.

Cerri S, Bohn MA, Menke K, Galfetti L (2009) Ageing behavior of HTPB based rocket propellant formulations. Cent Eur J Energ Mater 6(2):149-165.

Cerri S, Bohn MA, Menke K, Galfetti L (2013) Ageing of HTPB/AL/AP rocket propellant formulations investigated by DMA measurements. Propellants Explos Pyrotech 38(2):190-198. doi: 10.1002/prep.201200186

Davenas A (1993) Solid rocket propulsion technology. Oxford; New York: Pergamon Press.

Fluke GA (1969) Composite solid propellant processing techniques. In:

Boyars C, Klager K, editors. Propellants manufacture, hazards, and testing. Vol. 88. Washington: American Chemical Society. p. 165-187.

Hufferd WL, Fitzgerald JE (1976) Development of a solid propellant viscoelastic dynamic model. Atlanta: J. E. Fitzgerald & Associates.

Kubota N (2007) Propellants and explosives. Weinheim: Wiley-VCH Verlag GmbH & Co.

Lemos MF, Bohn MA (2016) Evaluation of the effect of plasticizers on the DMA loss factor, the thermal and mechanical properties of Desmophen® 2200-based elastomers used for composite propellants. Proceedings of the 18th International Seminar on New Trends in Research of Energetic Materials; Pardubice, Czech Republic.

Nardai MM, Bohn MA (2015) Cohesion properties in PBX and composite propellants – computational results and experimental aspects. Proceedings of the 46th International Annual Conference of ICT; Karlsruhe, Germany.

Ornaghi Jr HL, Bolner AS, Fiorio R, Zattera AJ, Amico SC (2010) Mechanical and dynamic mechanical analysis of hybrid composites molded by resin transfer molding. J Appl Polymer Sci 118(2):887-896. doi: 10.1002/app.32388